RSC Advances

Beaded Structured CNTs-Fe3O4@C with Low Fe3O4 Content as Anode Materials with Extra Enhanced Performances in Lithium ion Batteries

Journal:	*RSC Advances*
Manuscript ID:	RA-ART-01-2015-001262.R1
Article Type:	Paper
Date Submitted by the Author:	15-Mar-2015

Complete List of Authors:	Xu, Yuan; Changchun Institute of Applied Chemistry, Feng, Jingdong; Changchun Institute of Applied Chemistry, Chen, Xuecheng; Changchun Institute of Applied Chemistry, Kierzek, Krzysztof; Wroclaw University of Technology, Liu, Wen-bin; Harbin Engineering University, College of Materials Science and Chemical Engineering Tang, Tao; Changchun Institute of Applied Chemistry, Mijowska, Ewa; West Pomeranian University of Technology,

RSC Advance

RSC Publishing

ARTICLE

Beaded Structured CNTs-Fe_3O_4@C with Low Fe_3O_4 Content as Anode Materials with Extra Enhanced Performances in Lithium ion Batteries

Cite this: DOI: 10.1039/xoxxooooox

Received ooth January 2012,
Accepted ooth January 2012

DOI: 10.1039/xoxxooooox

www.rsc.org/

Yuan Xu[a,c], Jingdong Feng[a], Xuecheng Chen[a,b]*, Krzysztof Kierzek[d], Wenbin Liu[c]* and Tao Tang[a]*, Ewa Mijowska[b]

The present paper reports a facile method to synthesize CNT-Fe_2O_3 and CNTs-Fe_3O_4@C beaded structures by deposition of Fe_2O_3 and carbon layers on CNTs, which integrate both electronic conductivity and buffering matrix design strategies. The CNT-Fe_2O_3 and CNTs-Fe_3O_4@C were tested as anode materials for lithium-ion batteries, CNT-Fe_2O_3 showed excellent cycling performance, the reversible capacity retention after 80 cycles is stable at 410 mAh/g. However, CNTs-Fe_3O_4@C exhibited even improved reversible capacity and better cycling performance when compared to CNT and CNTs-Fe_2O_3. The highly improved reversible capacities are attributed to the combination of (a) the network structured CNTs, which improve the matrix electrical conductivity, (b) the mesopores created by carbon coating on Fe_3O_4 nanoparticles and CNTs, which increases lithium-ion mobility and storage, and (c) the Fe_3O_4 nanoparticles attached to the CNTs facilitate the transport of electrons and shorten the distance for Li^+ diffusion. This study provides a cost-effective, highly efficient method to fabricate nanomaterials which combine carbon nanotubes with iron oxide nanoparticles for the development of lithium ion battery with high-performance.

Introduction

Re-chargeable lithium-ion batteries are considered to be excellent power source for energy storage devices and they have great potential in portable electronic market,[1] thus various materials for electrodes of lithium-ion batteries have been intensely investigated. Ideal electrode materials for battery application should be cheap, nontoxic, have high energy and power densities (meaning high capacity and high rate performance) and last long cycles (meaning 100% Coulombic efficiency and stability of the electrochemical performance versus cycling).[2]

Among those, the iron oxides are one of the most promising candidates due to its abundance, low cost, chemical stability, and environmental friendliness. The Fe_3O_4 electrode has the higher theoretical reversible capacity (926 mAh/g). However, the Fe_3O_4 anode materials suffer from poor cyclic performance, which is mainly caused by its low conductivity and morphological collapse by the large volume changes during the charge/discharge cycles. Fabrication of iron oxides with carbon coating has been considered as one of the most effective ways towards high-performance electrode materials for lithium ion batteries, especially for the electrode materials with volume variation during the charge-discharge process.[3] Under the stimulus of this idea, various carbon-mixed Fe_3O_4 anode materials have been reported,[4-7] e.g. Fe_3O_4 nanorods, nanospindles, and nanowires have been coated by carbon shells and presented better electrochemical performance.[8-12] Carbon nanotubes (CNTs) are widely used in the field of preparation of hybrid electrode materials due to their excellent electrical conductivity. For example, Zhou et al. have prepared a nanosized Fe_2O_3 decorated single-walled carbon nanotubes as flexible anode for lithium ion batteries, showing a discharge capacity of 801 mAh/g after 90 cycles. The highly conducting SWCNT network in membrane not only facilitates electrons conduction of Fe_2O_3, but also buffers the strain of Fe_2O_3.[13] Park et. al also reported a novel structure of the CuO/CNT nanocomposite in which the mesoporous CuO particles were threaded by CNTs. The strong binding of the CuO to the CNTs and their micropores endowed morphological stability during the repeated battery cycles. The CNTs threading the CuO particles provided high electrical conductivity. The synergic effect of the morphological stability of the CuO particles and high conductivity by CNTs achieved significant advances in the cycling performance and the rate capabilities in lithium-ion batteries.[14] In addition to the well conductivity, CNTs also have other advantages in the application of electrode for lithium ion batteries. A stable solid electrolyte interphase (SEI) film could be formed during charge/discharge because the electrolytes will contact with the outer surface of CNTs. On the other hand, CNTs electrodes also can react with lithium ion at a lower potential and accommodate drastic volume variation during discharge–charge cycles due to its network structure.[15] For the lithium ion batteries, a rapid charge transfer process at the electrode surface is highly desired, implying the importance of a high surface area and electrical conductivity for anode materials.[16] Since high energy capacity depends on morphology, the anode rate capability can be improved by introducing macro/mesoporosity into carbon to form a highly porous structure.

In this article, we developed a new method to synthesize beaded structured CNT-Fe_2O_3 and CNTs-Fe_3O_4@C, which integrate both electronic conductivity, iron oxide nanoparticles and suitable mesopores created by carbon coating. The resulted CNTs-Fe_3O_4@C possesses good electronic conductivity, high specific surface areas and Fe_3O_4 nanoparticles attached on CNT. Both of CNT-Fe_2O_3 and CNT-Fe_3O_4@C were tested as anode materials for lithium-ion batteries, especially, CNT-Fe_3O_4@C exhibited higher capacity and more excellent cyclability compared to CNTs-Fe_2O_3 due to the extra lithium ion storage capacity from carbon coating.

Experimental Section

Materials

Carbon nanotubes were purchased from Shenzhen Nanoport Co., LTD, China (diameter: 20−40 nm). $FeCl_3$ and glucose were bought from Sigma-Aldrich, which were used directly without further purification. All other materials were of analytical grade and commercially available.

Functionalization of Carbon nanotubes

In a typical synthesis, 50 mg of carbon nanotubes was first dispersed into 300 mL of concentrated nitric acid (65 wt %) and refluxed at 130 °C in an oil bath for 36 h. After the mixture was cooled down to room temperature, it was diluted with distilled water and rinsed several times until the pH value reaches neutral. Then, the product was dried at 100 °C for further use.

Synthesis of CNT- Fe_2O_3

Typically, 50 mg of the above functionalized carbon nanotubes were dispersed in the 50 mL of 2.0×10^{-2} M $FeCl_3$ aqueous solution by sonication for 1 h. Afterwards, the hexahedral hematite particle decorated carbon nanotubes were obtained via refluxing the solution at 110 °C for 48 h.

Synthesis of CNT-Fe_3O_4@C

CNTs@Fe_3O_4@C beaded structures were prepared by a glucose hydrothermal process and subsequent carbonization process. Briefly, 50 mg CNT-Fe_2O_3 were dispersed in 25 mL 0.2 M aqueous glucose solution. After sonication for 30 min, the solution was transferred into a 50 mL Teflon-lined stainless steel autoclave, sealed, and maintained at 190 °C for 12 h. After the reaction was finished, the resulting black solid product was centrifuged, washed with distilled water and ethanol to remove the ions possibly remaining in the final products, and dried in a vacuum at 80 °C. Finally, the black product was kept in a tube furnace at 450 °C for 3 h under N_2 at a ramping rate of 5 °C/min.

Characterization

The morphology of the samples was observed by means of field-emission scanning electron microscope (SEM, XL30ESEM-FEG) and transmission electron microscope (TEM, JEM-1011) at an accelerating voltage of 100 kV. The phase structure was analyzed by X-ray diffraction (XRD) using a D8 advance X-ray diffractometer with Cu Kα radiation operating at 40 kV and 200 mA. The vibrational property was characterized by Raman spectroscopy (T6400, excitation-beam wavelength: 514.5 nm). The electrochemical experiments were carried out using 2032 coin-type cells. The working electrodes were prepared by mixing the beaded structures, carbon black (C-NERGY SUPER C65, Timcal), and polyvinylidene difluoride (PVDF, Solef 5130, Solvay) at a weight ratio of 80:10:10 and pasting onto Cu foils (Schlenk Metallfolien GmbH & Co.). A lithium foil (Aldrich) was used as the counter electrode. The electrolyte, consisted of a solution of 1 M LiPF6 in ethylene carbonate (EC)/dimethyl carbonate (DMC) (1:1 by volume), was obtained from Merck Chemicals (SelectiLyte LP30). The cells were assembled in an argon-filled glovebox with less than 1 ppm moisture and oxygen. The electrochemical performance was evaluated in the voltage range of 0.01−3.0 V by using a galvanostatic charge/discharge technique at a rate of C/10.

Results and Discussion

Herein, CNT-based hybrid nanostructures: CNT-Fe_2O_3 and CNTs-Fe_3O_4@C beaded structures were prepared by a sol-gel and subsequent hydrothermal carbonization process. First, carbon nanotubes were oxidized by concentrated HNO_3, forming –COOH groups on the surface of CNTs. In the next step, the carboxylic groups on the CNTs could attract and strongly bond with Fe^{3+} ions in $FeCl_3$ solution through electrostatic attractions. After this procedure, Fe_2O_3 nanoparticles are attached to the surfaces of the CNTs. Thereafter, a carbon layer with a desired thickness was deposited on the surface of the hematite core and CNTs. After calcination of the sample in N_2, the phase structure was changed from Fe_2O_3 to Fe_3O_4 due to reduction by CNTs.

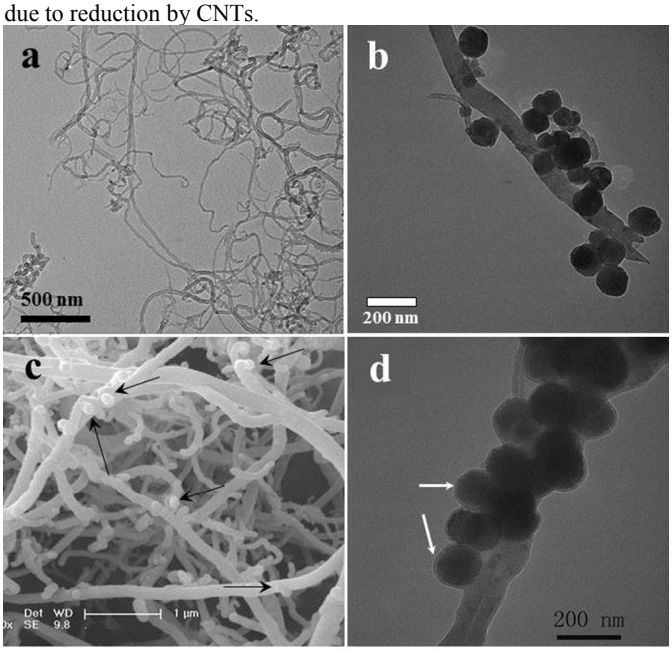

Figure 1. TEM images of original CNTs (a), CNT-Fe_2O_3 (b) and CNT-Fe_3O_4@C (c), and SEM image of CNT-Fe_3O_4@C (d).

The morphology of the samples in the starting, intermediate and final form is visualized by TEM and SEM images in Figure 1. The pristine CNTs with a smooth surface can be obviously observed in Figure 1a, whereas the CNT-Fe_2O_3 nanostructures exhibited a 1D hybrid structure and coarse surfaces (Figure 1b). There are some particles with diameter of around 150 nm attached on the surface of CNTs. In Figure 1d, CNTs-Fe_3O_4@C beaded structures have a uniform and continuous carbon layers of about 5-10 nm in thickness. Figure 1c shows SEM image of the CNTs-Fe_3O_4@C. On the surface of the fiber-like structures some particles can be found (as indicated by black arrows). Hydrothermal carbonization of saccharides (glucose, sucrose and starch) has been widely accepted as a facile route to prepare carbon-coated hybrid nanostructures.[17] The reaction parameters (glucose concentrations, hydrothermal temperature, and time) play important roles in the morphologies of final products. Therefore, CNTs@-Fe_3O_4@C beaded structures with controlled thickness of carbon layer can be easily obtained by adjusting hydrothermal time and glucose concentrations (as indicated by white arrows).

Figure 2 displays the XRD patterns of the pristine CNTs, Fe_2O_3-CNT and CNT-Fe_3O_4@C. In a pattern (a) the strong peak at 2θ = 26°, broad ones at 42.7°(2θ) and 43.9°(2θ)(marked with black filled

cube), are corresponding to the characteristic (002) and (100) diffraction peaks of CNTs (JCPDS 65-6212), respectively. In a pattern (b), the observed peaks (33.6, 36.1, 49.9, 54.5, 62.9, 64.4° (marked with red triangle)) are ascribed to α-Fe_2O_3 (JCPDS No. 72-00469) so the nanoparticles observed in TEM correspond to α-Fe_2O_3. As it can be seen in a pattern (c), a carbon layer was deposited on the surface of the hematite cores and carbon nanotubes. After annealing in N_2, it is evidenced by appearance of new diffraction peaks at 2θ = 30, 35.3, 43, 56, and 62° (marked with blue star), which means that Fe_2O_3 was reduced to Fe_3O_4. The peak of the CNT at 26° (2θ) is also observable in Fe_2O_3-CNT and CNT-Fe_3O_4@C samples. For the peak at 26°, the intensity of this peak is enhanced in CNT-Fe_3O_4@C in respect to Fe_2O_3-CNT. It means the carbon coating also carbonized to graphitic carbon in the presence of iron oxide.

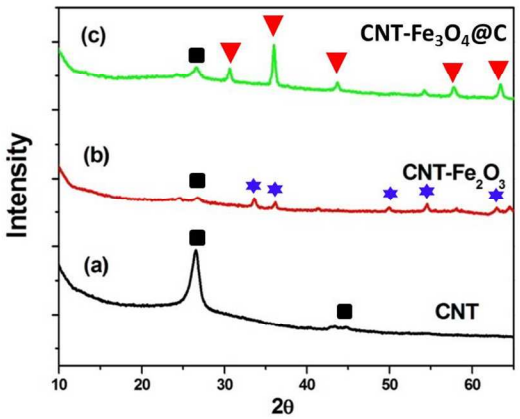

Figure 2. XRD patterns of CNT(■), CNT-Fe_2O_3 (▼) and CNT-Fe_3O_4@C (★).

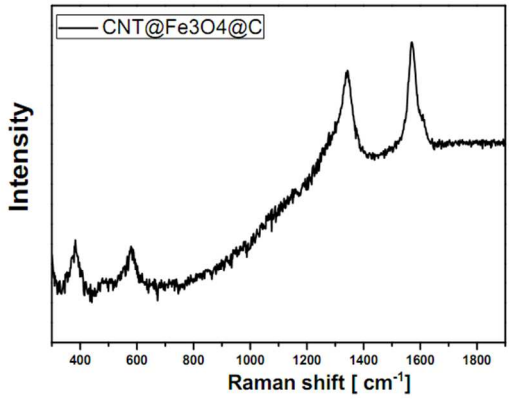

Figure 3. Raman spectra of CNT-Fe_3O_4@C beaded structures.

Figure 3 shows the Raman spectra of the CNT-Fe_3O_4@C. The peak at about 1580 cm^{-1} (G band) corresponds to an E_{2g} mode of hexagonal graphite and is related to the vibration of sp^2-bonded carbon atoms in a graphite layer, and the D band at about 1350 cm^{-1} is associated with vibration of carbon atoms with dangling bonds in the plane terminations of disordered graphite or glassy carbons. The I_D/I_G ratio indicates the predominantly amorphous/ordered nature of the CNT-Fe_3O_4@C, which was consistent of the results of XRD.

To investigate the porosity of the CNT-Fe_2O_3 and CNT-Fe_3O_4@C, the nitrogen sorption/desorption isotherms were measured. Figure 4a and 4b display the typical II isotherms of the hysteresis of porous system of CNT-Fe_2O_3 and CNT-Fe_3O_4@C beaded structures. Based on analysis on the adsorption branch of nitrogen sorption, the obtained specific surface areas (Brunauer–Emmett–Teller, (BET)) of CNT-Fe_2O_3 and CNT-Fe_3O_4@C are 49.2 and 232.6 m^2/g, respectively. The specific surface area of obtained CNT is 120.1 m^2/g. The specific surface area of CNT-Fe_3O_4@C is much larger than CNT-Fe_2O_3. The average pores diameter for CNT-Fe_3O_4@C beaded structures were determined as 1.1 and 1.9 nm. The specific surface area of CNT-Fe_3O_4@C increased when compared with CNT-Fe_2O_3. We suppose that the generated mesopores could influence the shrinkage of the carbon coating and re-crystallization of iron oxide during the heat treatment. During its carbonization process of CNT-Fe_2O_3 coated with amorphous carbon layer, , the Fe(III) can be partially reduced to Fe(II) by the carbon layer, which together with the loss of water molecules could lead to the formation of empty pores in the crystal structure.[18]

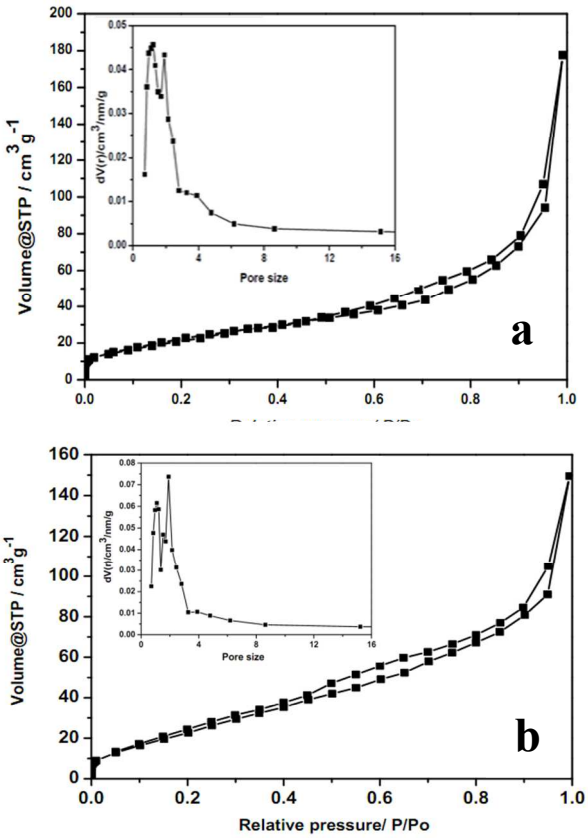

Figure 4. N_2 sorption/desorption isotherms of CNT-Fe_2O_3, CNT-Fe_3O_4@C and corresponding pore size distributions.

As shown in Figure 5, TGA were used to measure the weight loss of CNT, CNT-Fe_2O_3 and CNT-Fe_3O_4@C composite when burnt in air conditions. For these three samples, the weight losses from CNT mainly took place between 300 and 700 °C. For pure CNT, it began to pyrolyze at 550 °C. However, after supporting of Fe_2O_3 and Fe_3O_4 nanoparticles, the stability of CNT-Fe_2O_3 is dropped in respect to the pure CNT. As observed, the sample of CNT-Fe_2O_3 began to decompose at 200 °C. For these three samples, the iron oxide contents were 0, 50 and 21.6 wt% at 900 °C for CNT, CNT-Fe_2O_3 and CNT-Fe_3O_4@C, respectively. So for the sample of CNT-Fe_3O_4@C, there is less than 21 wt % of Fe_3O_4 existed in CNT-Fe_3O_4@C composite.

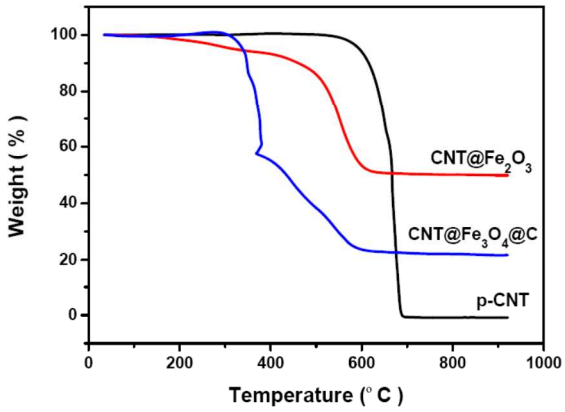

Figure 5. TGA profiles of CNT, CNT-Fe_2O_3 and CNT-Fe_3O_4@C composites.

To investigate and compare the impact of the unique structure of CNT-Fe_2O_3 and CNT-Fe_3O_4@C on lithium storage capabilities, all the coin cells were assembled and test under the same conditions. The curves of capacity versus cycle number at current density of C/10 for CNT-Fe_2O_3 and CNT-Fe_3O_4@C were shown in Figure 6. As presented in Figure 6 a, the sample of CNT-Fe_2O_3exhibited excellent cycling performances. After 80 cycles, the recharge capacity retention is stable at 410 mAh/g, which is even higher than the initial reversible capacity. This proved that the advantages of beaded structured CNT-Fe_2O_3 in lithium ion batteries. The rate performances of the pure CNT were also shown in Figure 6 b. Here, with the rate of C/10 after 30 cycles, the reversible capacity is stable at 218 mAh/g. So, for the sample of CNT-Fe_2O_3, the contribution to the recharge capacity retention from CNT is only around 100 mAh/g. However, after coating with carbon layers, for the sample of CNT-Fe_3O_4@C beaded structures, the first discharge capacity is 1543 mAh/g, which is much higher than that of CNT-Fe_2O_3 with discharge capacities of 1100 mAh/g (see Figure 6 c). Despite the capacity decayed in the first cycle, even after 80 cycles, the discharge capacity still retain at a value of 720 mAh/g. This is also much higher than of CNT-Fe_2O_3 (410 mAh/g). As we can see the performances of CNT in lithium ion battery, the large capacity of CNT-Fe_2O_3 and CNT-Fe_3O_4@C is supposed to be attributed mainly to iron oxide. However, as reported in the literature,[19] the first discharge capacity of commercial Fe_3O_4 nanoparticle electrode is measured at 1035 mAh/g. After 30 cycles, the discharge capacity of electrode rapidly decreased to 106 mAh/g. For the sample of CNT-Fe_3O_4@C, the contribution of Fe_3O_4 is less than 203 mAh/g. Basing on above-mentioned results, the good cycling performances of CNT-Fe_3O_4@C are mainly derived from coating with carbon layer, what could deliver more pores to afford more lithium ions stored in CNT-Fe_3O_4@C composite, leading to enhanced electrochemical performances. This is also confirmed by N_2 sorption/desorption results of CNT-Fe_3O_4@C, the specific surface area of CNT-Fe_3O_4@C (232.6 m^2/g) is much larger than CNT-Fe_2O_3 (49.2 m^2/g), indicating more mesopores are produced after carbon coating. TEM image of CNT-Fe_3O_4@C also confirmed this conclusion (Figure 7), as indicated by white arrows, there are many holes existed in the Fe_3O_4 particles. The irreversible capacity loss in the first cycle can be attributed to the formation of a solid electrolyte interphase (SEI) film, the decomposition of the electrolyte, and the reaction of the oxygen-containing functional groups on the outer carbon/ inner CNT with lithium ions. Furthermore, a stable SEI film can form on the formed carbon layer. Thus, combined with the excellent conductive performance of CNT, mechanical strength of carbon layer the sample of CNT-Fe_3O_4@C exhibited higher and stable cyclability than CNT-Fe_2O_3 composite.

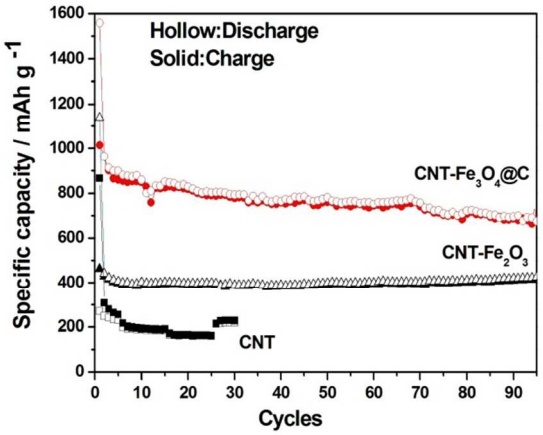

Figure 6. Cycling performances of CNT-Fe_2O_3 and CNT-Fe_3O_4@C beaded structures and rate performances of CNTs.

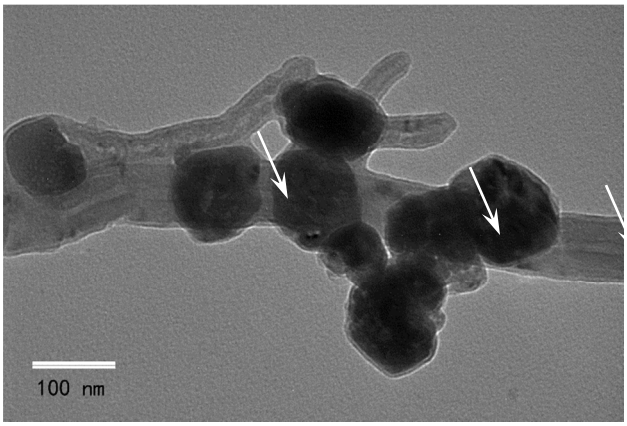

Figure 7. High resolution TEM image of CNT-Fe_3O_4@C.

To present the advantage of coating of the sample with carbon layer, the lithium insertion/extraction processes in the CNT-Fe_2O_3 and the CNT-Fe_3O_4@C nanocomposite were further characterized by cyclic voltammetry (CV) in Figure 8. A cathodic peaks in the range of 0.72-0.75 V can be attributed to the solid electrolyte interphase (SEI) formation on the external surface of the materials or/and electrochemical iron oxide reduction. The peak at 0.85V is during 2nd cycle when the SEI should be already formed. A couple 0.85V/1.67V probably comes from insertion/deinsertion of Li in iron oxide; couple 0.01V/0.16V – from carbon phase. After coating with carbon layer, as shown in Figure 7b, the peak at 0.85 became very weak as an effect of lower contribution of iron oxide. A low cathodic current at 0.75V means that the carbon coating can weaken the formation of SEI film and form strong thin layer structured SEI. This kind of shell is favored for the lithium ions transported in it and it made beaded structured CNT-Fe_3O_4@C more stable.

Several advantages can be expected from this nanostructure. The porosity of the Fe_3O_4 particles allows easy access of Li ions and carbon layer not only plays as an elastic buffer for the volume change during lithiation/delithiation process but also provides an extra open space for lithium ion storage. The CNTs enhance the electronic conductivity of the nanocomposite and the long-term

stability of the anodes. The anode materials are fully confined between CNTs and carbon layer, which can effectively preserve the nanostructure during the cycling. The anodes showed remarkable advances in the electrochemical performances, including a high reversible capacity (720 mAh/g at 1/10 C) and stable capacity retention (100% in 80 cycles).

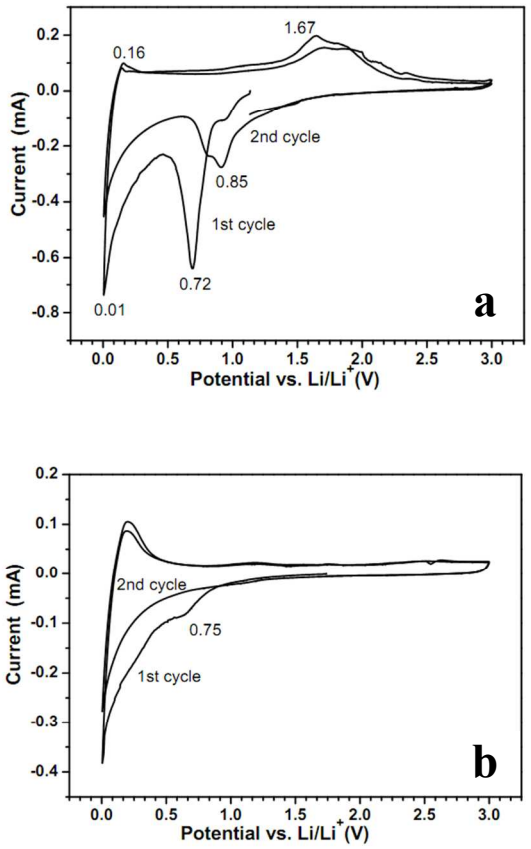

Figure 8. CV curves of (a) CNT-Fe_2O_3 and (b) CNT-Fe_3O_4@C beaded structures.

Conclusions

A simple, effective and reproducible method has been carried out for synthesis of CNT-Fe_2O_3 and CNT-Fe_3O_4@C beaded structures. As anode materials for lithium ion batteries, CNT-Fe_2O_3 showed excellent cycling performance, the reversible capacity retention after 80 cycles is stable at 410 mAh/g. However, for CNT-Fe_3O_4@C sample, firstly carbon coating could make Fe_3O_4 nanoparticles strongly attach to the CNTs and accommodate the volume changes of Fe_3O_4 during charge-discharge process, secondly it can create extra mesopores, which increased the specific surface areas of CNT-Fe_3O_4@C composite. The initial discharge and charge capacity of The CNT-Fe_3O_4@C nanocomposite electrode are 1558 mAh/g and 1012 mAh/g, respectively. The recharge capacity retention after 80 cycles remains 720 mAh/g, which is significantly higher than that of the commercial graphite material. The excellent cyclebility and the high capacity retention of the electrodes are attributed to the combined effects of uniformly dispersed Fe_3O_4 nanoparticles, highly strong network as well as facilitation of electron transfer contributed by CNTs and carbon coating on the Fe_3O_4 particles on CNTs. Most importantly, high BET areas from carbon layer coating also can improve the cycling performances of CNT-Fe_3O_4@C when compared with CNT-Fe_2O_3, which mainly contributed from extra mesopores created by carbon coating.

Acknowledgements

This work was supported by the Chinese National Science within the project No. 51303170, National Science Centre, Poland within the project SONATA BIS UMO-2012/07/E/ST8/01702.

Notes and references

[a] State Key Laboratory of Polymer Physics and Chemistry, Changchun Institute of Applied Chemistry, Chinese Academy of Science (CAS), Renmin Road 5625, 130022, Changchun, China. E-mail: xchen@ciac.ac.cn; ttang@ciac.ac.cn

[b] Institute of Chemical and Environment Engineering, West Pomeranian University of Technology, 70-322, Szczecin, Poland.

[c] Department of Polymer and Carbonaceous Materials, Wroclaw University of Technology, ul. Gdanska 7/9, 50-344 Wroclaw, Poland.

[d] Polymer Materials Research Center, College of Materials Science and Chemical Engineering, Harbin Engineering University, Harbin 150001, China. E-mail: wjlwb@163.com

1 (a) M. Armand, J. M. Tarascon, *Nature,* 2008, **451**, 652-657. (b) P. G. Bruce, B. Scrosati, J. M. Tarascon, *Angew. Chem. Int. Ed.,* 2008, **47**, 2930. (c) B. J. Landi, M. J. Ganter, C. D. Cress, R. A. Dileo, R. P. Raffaelle, *Energy. Environ. Sci.,* 2009, **2**, 638-654.

2 (a) Y. G. Guo, J. S. Hu, L. J. Wan, *Adv. Mater.,* 2008, **20**, 2878-2887. (b) F. Y. Cheng, J. Liang, Z. L. Tao, J. Chen, *Adv. Mater.,* 2011, **23**, 1695-1715. (c) J. B. Goodenough, Y. Kim, *Chem. Mater.,* 2010, **22**, 587-603.

3 Z. S. Wu, G. M. Zhou, L. C. Yin, W. C. Ren, F. Li, H. M. Cheng, *Nano Energy,* 2012, **1**, 107–131.

4 F. Han, D. Li, W. C. Li, C. Lei, Q. Sun, A. H. Lu, *Adv. Funct. Mater.,* 2013, **23**, 1692–1700.

5 Y. Li, C. L. Zhu, T. Lu, Z. P. Guo, D. Zhang, J. Ma, S. M. Zhu, *Carbon,* 2013, **52**, 565–573.

6 L. W. Ji, O. Toprakci, M. Alcoutlabi, Y. F. Yao, Y. Li, S. Zhang, B. K. Guo, Z. Lin, X. W. Zhang, *ACS Applied Materials & Interface,* 2012, **4**, 2672–2679.

7 C. N. He, S. Wu, N. Q. Zhao, C. S. Shi, E. Z. Liu, J. J. Li, *ACS Nano,* 2013, **7**, 4459–4469.

8 T. Muraliganth, A. V. Murugan, A. Manthiram, *Chem. Commun.,* 2009, **45**, 7360-7362.

9 H. Liu, G. X. Wang, J. Z. Wang, D. Wexler, *Electrochem. Commun.,* 2008, **10**, 1879-1882.

10 W. M. Zhang, X. L.Wu, J. S. Hu, Y. G. Guo, L. J. Wan, *Adv. Funct. Mater.,* 2008, **18**, 3941-3946.

11 Y. Z. Piao, H. S. Kim, Y. E. Sung, T. Hyeon, *Chem. Commun.,* 2010, **46**, 118-120.

12 C. M. Ban, Z. C. Wu, D. T. Gillaspie, L. Chen, Yan, Y. F.; Blackburn, J. L.; Dillon, A. C. *Adv. Mater.* 2010, **22**, E145-149.

13 G. M. Zhou, D. W. Wang, P. X. Hou, W. S. Li, N. Li, C. Liu, F. Li, H. M. Cheng, *J. Mater. Chem.,* 2012, **22**, 17942–17946.

14 S. W. Ko, J. I. Lee, H. S. Yang, S. Park, U. Jeong, *Adv. Mater.,* 2012, **24**, 4451–4456.

15 Y. Wu, Y.Wei, J. Wang, K. Jiang, S. S. Fan, *Nano. Lett.,* 2013, **13**, 818–823.

16 (a) J. R. Dahn, T. Zheng, Y. Liu, J. S. Xue, *Science,* 1995, **270**, 590–3. (b) M. Winter, J. O. Besenhard, M. E. Spahr, P. Novak, *Adv. Mater.,* 1998, **10**, 725–63. (c) H. Zhou, S. Zhu, M. Hibino, I. Honma, M. Ichihara, *Adv. Mater.,* 2003, **15**, 2107–11. (c) F. Bonino, S. Brutti, P. Reale, B. Scrosati, L. Gherghel, J. Wu, *Adv. Mater.,* 2005, **17**, 743–6. (d) T. Renouard, L. Gherghel, M. Wachtler, F. Bonino, B. Scrosati, R. Nuffer, *J. Power Sources,* 2005, **139**, 242–349. (e) M. S. Kim, B. Fang, J. H. Kim, D. Yang, Y. K. Kim, T. S. Bae, *J. Mater. Chem.,* 2011, **21**, 19362–19367.

17 L. B. Luo, S. H. Yu, H. S. Qian, J. Y. Gong, *Chem. Commun.,* 2006, 793-795.

18 Y. Piao, J. Kim, H. Bin Na, D. Kim, J. S. Baek, M. K. Ko, J. H. Lee, M. Shokouhimehr, T. Hyeon, *Nat. Mater.,* 2008, **7**, 242–247.

19 T. Yoon, J. Kim, J. K. Lee, *Energies,* 2013, **6**, 4830-4840.

Table of Content

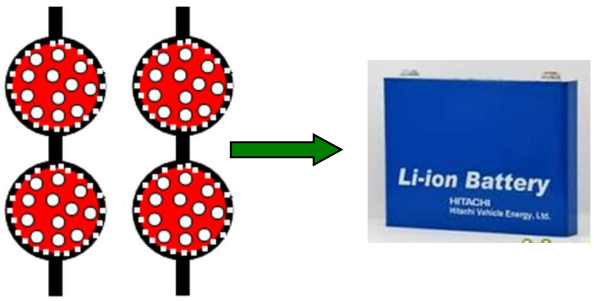

CNT-Fe_3O_4@C

A simple, effective and reproducible method has been carried out for synthesis of CNT-Fe_2O_3 and CNT-Fe_3O_4@C beaded structures for lithium ion battery.